IEEE Access
Multidisciplinary : Rapid Review : Open Access Journal

Received 10 April 2023, accepted 27 April 2023, date of publication 8 May 2023, date of current version 12 May 2023.

Digital Object Identifier 10.1109/ACCESS.2023.3273901

RESEARCH ARTICLE

An Analytical Formulation for Mapping the Spatial Distribution of Nodal Inertia in Power Systems

BRUNO PINHEIRO[1], (Graduate Student Member, IEEE), LUIGI VIOLA[1], (Graduate Student Member, IEEE), JOE H. CHOW[2], (Life Fellow, IEEE), AND DANIEL DOTTA[1], (Member, IEEE)

[1]Department of Electrical Engineering, University of Campinas—UNICAMP, Campinas, São Paulo 13083-852, Brazil
[2]Department of Electrical Computer and Systems Engineering, Rensselaer Polytechnic Institute, Troy, NY 12180, USA

Corresponding author: Bruno Pinheiro (b229989@dac.unicamp.br)

This work was supported in part by Engie, sponsor of this research developed under the Research and Development Program regulated by the Brazilian Electricity Regulatory Agency (ANEEL) under Grant PD-00403-0053/2021, and in part by the Brazilian Agency Coordination for the Improvement of Higher Education Personnel (CAPES) under Grant 88887.341682/2019-00 and Grant 88887.655531/2021-00.

ABSTRACT Mapping the spatial distribution of nodal inertia is crucial for helping system operators identify locational frequency stability issues in the power system operation planning process. Currently, index-based methods cannot retrieve the nodal inertia values for all load buses. To do so, this paper proposes an accurate analytical formulation relying only on steady-state system parameters to determine the nodal inertia values and, thus, map the spatial distribution of system inertia. The performance and reproducibility of the proposed formulation are evaluated using three test systems: a 5-bus radial system with two synchronous generators, a multimachine IEEE 68-bus benchmark system, and a larger NPCC 140-bus test system. We validate the proposed spatial distribution of nodal inertia using time-domain simulations and numerical estimations. In addition, we compare our method against the inertia distribution indexes presented in the literature. The results indicate that our formulation adequately quantifies the nodal inertia value in system buses, with low computational cost, and providing a suitable tool for operation planning analysis.

INDEX TERMS Nodal inertia, inertia distribution, locational stability, frequency stability, power system dynamics.

I. INTRODUCTION

A. MOTIVATION

One of the critical challenges in power systems operation planning with high penetration of inverter-based resources (IBRs) is the decrease in system inertia, which results in a high initial rate of change of frequency (ROCOF) [1]. Furthermore, recent theoretical studies [2], [3], [4] and data-driven analyzes [5], [6], [7] have shown that inertia providers are unevenly distributed across the system, and the frequency response after a disturbance has spatial-temporal characteristics. The practical problem is the unexpected tripping of ROCOF-based protection and triggering of under-frequency load shedding (UFLS) schemes at specific locations [8], [9].

In recent years, several works have been conducted in the industry and academia to detect and quantify different levels of inertia across power systems using real-time measurements [10]. The main idea is to use available synchrophasor measurements to estimate the equivalent [11], regional [12], and distributed inertia [13], [14], [15]. The results are promising, and industrial applications are already operating in control centers, particularly equivalent and regional inertia estimation approaches. However, these methodologies are employed in real-time operations and may not be helpful for power system operation planning that strongly relies on power system models. Thus, there is a clear need to develop analytical methodologies to identify and quantify

The associate editor coordinating the review of this manuscript and approving it for publication was Youngjin Kim.

This work is licensed under a Creative Commons Attribution-NonCommercial-NoDerivatives 4.0 License.
For more information, see https://creativecommons.org/licenses/by-nc-nd/4.0/

the locational lack of inertial resources in modern power systems, thereby improving the operation planning process and addressing problems such as optimal generation scheduling [16], [17] and allocation of inertial sources [18], [19].

B. LITERATURE REVIEW

Refining the system frequency response information to make it more granular is essential for enhancing locational frequency stability. The spatial distribution of nodal inertia and its applicability has recently been investigated in several studies [13], [14], [15], [20], [21], [22], [23], [24]. These studies can be divided into two categories based on the level of detail of the model: (*i*) dynamic models [20], [21], [22], [23], [24] and (*ii*) static models [2], [15], [25].

In the first approach, conventional nonlinear time-domain or linear simulations are explored using full dynamic models. Regarding the nonlinear time-domain simulation method, the authors in [20] aim to determine the inertia distribution by comparing the difference in each bus frequency with the frequency of the system center of inertia (COI) calculated during transient events. In this sense, they proposed an inertia distribution index that is correlated with the location of the system COI. Buses near the system COI have higher inertial responses than those far from the system COI and are subject to higher frequency variations [20], [26]. In [27], the index proposed in [20] is applied for placing actuators in a meshed system, aiming to enhance the power system stability. In [28] and [29], the inertia distribution index was used as a metric to adequately place the resources capable of providing fast frequency response. However, the need to carry out several time-domain simulations is computationally intensive [21], [27], particularly for meshed systems, where the location of the disturbance directly affects the index.

Using linear models, the authors in [23] and [24] explore the correlation between the dominant oscillation mode and inertia distribution, introducing a modal-based index that uses the sensitivity of the bus voltage angles and mode shape of the identified critical inter-area mode. The concept of sensitivity of network variables (voltage bus, angle bus, and line current) is applied to analyze the propagation of electromechanical oscillations after disturbances [30], guiding the description of the influence of a particular mode on the grid variables. Thus, [23] proposed a novel interpretation of the sensitivity of network variables by associating it with the spatial distribution of the nodal inertia. Although this formulation avoids time-domain simulations, it requires a linear dynamic model of the system, which may be subject to the complexities associated with the modeling of generators and their controllers. Additionally, the efficiency of this analytical index in a meshed system with various inter-area and local modes has not been addressed.

In the second approach, the authors relied on the network topology and inertia source locations to analyze the spatial-temporal frequency variations. In [2], the propagation of disturbances through the system from the ROCOF perspective was investigated. The authors showed the relationship between the disturbance propagation and spectral analysis of the Laplacian matrix of the system. In this sense, [25] proposed an evaluation of frequency stability using clusters based on the Fiedler vector, that is, the eigenvector related to the lowest non-zero mode of the Laplacian matrix. In both works, the authors explore the properties of the Laplacian matrix to identify and evaluate the locational frequency stability. In [15], the authors proposed an analytical formulation based on generator inertia and frequency participation factor [31] to validate their data-driven inertia distribution estimation. However, the derived formulation does not consider the system topology parameters and magnitude of the disturbance, which may affect the explicit calculation of nodal inertia.

None of these works can explicitly calculate the spatial distribution of nodal inertia. The works that rely on full dynamic models are limited to indexes that do not directly quantify the lack or excess of the nodal inertia resources. Full dynamic models are also complex, with strong parameter uncertainties depending on the planning process phase. The existing static models are limited to specific problems and may require further work to be applied to other planning applications.

C. CONTRIBUTIONS

In this paper, we propose a new analytical model that determines the value of the nodal inertia of each system bus. Explicitly finding the inertia value is more accurate than the approximation of current index-based methods and is readily understood by system operators. By mapping the nodal inertia, a visual spatial distribution facilitates the identification of inertia scarcity, supporting potential correction actions. Since our methodology is based on steady-state parameters, it avoids complex analysis and can be reproduced in different power systems with low computational cost.

Therefore, the main contributions of this paper are summarized as follows:

- A new and accurate analytical formulation to quantify the value of nodal inertia of power system buses as an alternative to index-based methods.
- Since our formulation depends only on steady-state parameters, the methodology is replicable and requires low computational effort, regardless of the different types of generator and control models and the network size.
- Our approach allows a straightforward analysis of the results from the mapping of system inertia, serving as a tool for system operators in operation planning studies, enabling actions to improve the locational frequency stability.

D. ORGANIZATION

The remainder of this paper is organized as follows. Section II introduces the concepts of frequency dynamics in

power systems and challenges in determining an analytical expression for the spatial distribution of nodal inertia. Section III introduces the proposed formulation, and in Section IV it is tested in three systems: a 5-bus radial, IEEE 68-bus system, and the NPCC 140-bus system. The main parameters affecting the spatial distribution of the inertia are investigated. The results are validated through time domain simulations. Section V compares existing inertia distribution indexes (time-domain and modal analysis-based). In addition, the consistency of the spatial distribution of inertia using our formulation is validated by considering the total inertia of the slow coherency areas. Section VI discusses the potential applications of nodal inertia knowledge. Finally, the conclusions are summarized in Section VII.

II. THEORETICAL BACKGROUND

A. SWING EQUATION AND RoCoF

The frequency dynamics after a power imbalance for a synchronous generator i are described by a first-order differential equation, as shown in (1) [32]:

$$2H_i \frac{d\Delta\omega_i(t)}{dt} = \Delta P_{m_i}(t) - \Delta P_{e_i}(t) - D_i \Delta\omega_i(t) \tag{1}$$

where H_i is the inertia constant, D_i is the load damping coefficient, Δ denotes variations from the equilibrium values, ω_i is the angular rotor speed, P_{m_i} is the mechanical power supplied in generator i, and P_{e_i} is the electrical power output of generator i. The inertia constant represents the kinetic energy stored in the rotating masses normalized by the nominal power of the generators.

During the inertial response period (i.e., the first seconds after contingency), variations in the mechanical power can be neglected [32], [33]. Considering $\Delta\omega(0^+) = 0$, the synchronous generator rate of change of frequency (RoCoF) is determined by (2).

$$\left.\frac{d\omega_i(t)}{dt}\right|_{t=0^+} = -\left.\frac{\Delta P_{e_i}(t)}{2H_i}\right|_{t=0^+} \tag{2}$$

The magnitude of the RoCoF is inversely proportional to the generator's inertia constant, which means that lower values of the inertia constant result in higher RoCoF values. Moreover, the RoCoF is proportional to the generator's electrical power deviation after a contingency.

B. CENTER OF INERTIA

During the transient period, the dynamic behavior of the synchronous generators is not necessarily the same. To formulate the swing equation for a multimachine power system, the aggregate generator model uses an equivalent generating unit that represents the average frequency response of all the generators [31]. The equivalent generating unit defines the center of inertia (COI) frequency

$$\Delta\omega_{COI} = \left(\sum_{i=1}^{n_g} H_i \Delta\omega_i\right) \Big/ \sum_{i=1}^{n_g} H_i \tag{3}$$

The frequency of COI is a theoretical reference, and it may not correspond to any physical point in the system [34]. However, system buses with frequency responses closer to the COI's frequency behavior have fewer oscillations after a disturbance [20], [23].

C. BUS FREQUENCY

To derive a formulation that allows an estimation of the inertia value at power system buses, we first consider the estimation of the frequency through the *frequency divider formula* (FDF) proposed in [31]:

$$\Delta \boldsymbol{f}_b(t) = D\Delta\boldsymbol{\omega}_g(t) \tag{4}$$

From (4), the frequency variations of power system buses ($\Delta f_b(t)$) are estimated using the rotor speeds of the synchronous generators ($\Delta\omega_g(t)$) and considering the system topology through the *frequency divider matrix* (D), obtained as

$$D = -B_{ext}^{-1} B_g \tag{5}$$

where the matrix $B_{ext} = \mathrm{Im}\{Y_{ext}\} \in \mathbb{R}^{n_b \times n_b}$, and Y_{ext} is the extended admittance matrix commonly used in fault analysis that comprises the standard admittance matrix with the internal reactances of synchronous generators. In addition, $B_g = \mathrm{Im}\{Y_g\} \in \mathbb{R}^{n_b \times n_g}$, and Y_g is the admittance matrix of the internal reactances of the synchronous generators. The matrix $D \in \mathbb{R}^{n_g \times n_b}$ is full rank and indicates the participation of all synchronous generators in the frequency variations at the system buses.

D. INERTIA DISTRIBUTION

The dynamic frequency behavior of a large-scale power system has a spatial-temporal characteristics. According to (4), this behavior is directly correlated with the electromechanical dynamics of the synchronous generators connected to the system. In this sense, after a disturbance, any system bus will have a dynamic frequency behavior similar to that of synchronous generators, including an initial resistance to frequency variations after disturbances, that is, inertial response (neglecting transient responses). Therefore, the inertia distribution problem assumes that a particular bus j, despite not having an inertial response source connected to it, receives the contribution of the inertia constants of all generators connected to the system. The main question is how to quantify these contributions for all system buses and thus obtain the spatial inertia distribution.

The underlying formulation for the inertia distribution problem can be obtained using equation (2), applied to consider the inertia contribution at a particular bus j. Considering the critical case where a disturbance ΔP_L^j is applied in a bus j at time $t = 0$, a fictitious inertia can be represented by [15]

$$h_j = \Delta P_L^j \Big/ \left(2 \left.\frac{df_j(t)}{dt}\right|_{t=0^+}\right) \tag{6}$$

where f_j is the frequency of bus j, ΔP_L^j is the magnitude of the disturbance at bus j, and h_j is the inertia at bus j.

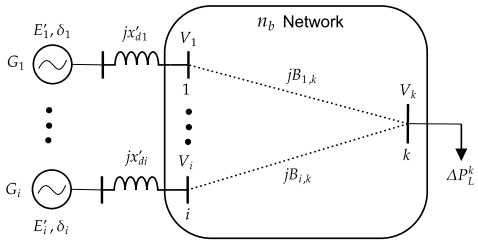

FIGURE 1. A system with n_b buses, internal machine buses and transient reactances (x'_{di}) and a power disturbance at bus k [32].

Considering that the network topology and generators are constant parameters, the derivative of (4) with respect to time results in the relationship between the frequency of system buses and the swing equations of synchronous generators, as [15]

$$\frac{d}{dt}\Delta \boldsymbol{f}_b(t) = D\frac{d}{dt}\Delta \boldsymbol{\omega}_g(t) \tag{7}$$

For the time $t = 0^+$, equation (7) is rewritten considering the formulation for a particular bus j as

$$\left.\frac{df_j(t)}{dt}\right|_{t=0^+} = -\sum_{i=1}^{n_g} \frac{D_{j,i}}{2H_i}\Delta P_{e_i}(0^+) \tag{8}$$

Note that the RoCoF at bus j depends on the inertial response of all synchronous generators in the system and their respective active power magnitudes immediately after the disturbance. From the underlying equation (6), the RoCoF of bus j can be written as [15].

$$\frac{\Delta P_L^j}{h_j} = \sum_{i=1}^{n_g} \frac{D_{j,i}}{H_i}\Delta P_{e_i}(0^+) \tag{9}$$

To find the values of $\Delta P_{e_i}(0^+)$ that are dependent on ΔP_L^j, it is necessary to use dynamic simulations. To avoid this, the authors in [15] consider $\Delta P_{e_i}(0^+) = \Delta P_L^j = 1$ pu as a reasonable approximation. Therefore, the inertia at each bus of the system is calculated as shown in (10).

$$h_j = \frac{1}{\sum_{i=1}^{n_g} \frac{D_{j,i}}{H_i}} \tag{10}$$

However, the individual power mismatch of synchronous generators is not the same at the moment of disturbance, and the approximation $\Delta P_{e_i}(0^+) = 1\ pu$ may not be valid for all cases, thereby harming the accuracy of the system inertia distribution mapping. To overcome this issue, we propose a new analytical formulation to determine the exact inertia distribution, that is, the value of inertia in all buses of the system.

III. ANALYTICAL FORMULATION

A. DISTRIBUTION OF POWER IMPACTS

In a multimachine power system with n_g synchronous generators, the linearized electrical power output of a generator i, following a change in $\delta_{i,j}$ regarding an initial steady-state condition $\delta_{i,j0}$, is described as [32]:

$$\Delta P_{e_i} = \sum_{\substack{j=1 \\ j\neq i}}^{n_g} K_{i,j}\Delta\delta_{i,j} \tag{11}$$

where $\delta_{i,j}$ is the angle difference between the internal buses of generators i and j, and the term $K_{i,j}$ is called the synchronizing power coefficient between generators i and j, which is calculated as

$$K_{i,j} = E_iE_j(B_{i,j}\cos\delta_{i,j0} - G_{i,j}\sin\delta_{i,j0}) \tag{12}$$

Here E_i and E_j are magnitudes of the internal voltages of the generators on buses i and j, respectively, $G_{i,j} = \mathrm{Re}\{Y_{i,j}^{\mathrm{red}}\} \in \mathbb{R}^{n_g\times n_g}$ and $B_{i,j} = \mathrm{Im}\{Y_{i,j}^{\mathrm{red}}\} \in \mathbb{R}^{n_g\times n_g}$, are the real and imaginary elements of the system admittance matrix reduced to internal generator nodes ($Y_{i,j}^{\mathrm{red}}$), for buses i and j.

This concept can be extended when a sudden load disturbance ΔP_L^k is applied at bus k in the transmission system, as shown in Figure 1, where $x'd_i, E_i, \delta_i$ are internal parameters of generator i. In this case, the network is reduced to the internal machine buses and the node k ($Y_k^{\mathrm{red}} \in \mathbb{C}^{n_g+1}$) [32]. Immediately after the perturbation ($t = 0^+$), the electrical active power output of generator i is approximated as a function of total disturbance ΔP_L^k, as shown in (13) [32]:

$$\Delta P_{e_i}(0^+) = \left(K_{i,k} \Big/ \sum_{j=1,}^{n_g} K_{j,k}\right)\Delta P_L^k \tag{13}$$

where ($K_{i,k}$) is the synchronizing power coefficient between generator i and bus k and is defined as

$$K_{i,k} = E_iV_k(B_{i,k}^k\cos(\delta_{i0} - \theta_{k0}) - G_{i,k}^k\sin(\delta_{i0} - \theta_{k0})) \tag{14}$$

Here, V_k and θ_{k0} are the voltage magnitude and voltage angle of bus k, respectively. Notice that $B_{i,k}^k$ and $G_{i,k}^k$ now refers to the reduced matrix with the disturbed bus k, i.e., elements of $Y_k^{\mathrm{red}} \in \mathbb{C}^{(n_g+1)\times(n_g+1)}$.

Therefore, the active power imbalances resulting from the disturbance is distributed throughout all generators in the system by synchronizing power coefficients between i and k, with $i = 1, 2\ldots, n_g$. Consequently, the impact of a load disturbance relies on the steady-state conditions and the location of the contingency [32], [35], and must be considered in the inertia distribution formulation.

B. PROPOSED INERTIA DISTRIBUTION FORMULATION

In order to properly quantify the inertia distributed to a bus j, equation (13) is applied to (9), leading to the elimination of the dependency of $\Delta P_{e_i}(0^+)$ and ΔP_L^j in the underlying formulation (9). Thus, the inertia distribution is written as a function of synchronizing power coefficients:

$$\frac{1}{h_j} = \frac{1}{\left(\sum_{k=1}^{n_g} K_{k,j}\right)} \sum_{i=1}^{n_g} \frac{D_{j,i}K_{i,j}}{H_i} \tag{15}$$

Hence, using equation (12) and assuming a high $X_{i,j}/R_{i,j}$ ratio at the transmission level, where $G_{i,j} \approx 0$, the inertia distribution formulation is finally obtained as,

$$h_j = \frac{\sum_{k=1}^{n_g} B_{k,j} E_k \cos(\delta_{k0} - \theta_{j0})}{\sum_{i=1}^{n_g} \left(\frac{D_{j,i}}{H_i}\right) B_{i,j} E_i \cos(\delta_{i0} - \theta_{j0})} \tag{16}$$

Note that in contrast to the approximated formulation in (10), the inertia distribution equation in (16) properly includes the behavior of synchronous generators' active power through steady-state conditions and its electrical distance to the particular bus. Therefore, the quantification of the inertia for each system bus is obtained considering two terms: the first takes into account the contributions of each generator inertia constant (H_i), as well as its participation in frequency bus behavior through the $D_{i,j}$ factor. The second handles the total electrical distance between the generators and the particular bus j, that is, the total resistance through ($\sum_{k=1}^{n_g} B_{k,j}$). The value of inertia obtained for each bus reflects the contribution of all synchronous generators to the local inertial response. Therefore, this value is limited to the total inertia of the system.

Figure 2 summarizes the steps to calculate the nodal inertia for a generic bus j. Extending the these steps to determine the nodal inertia of all system buses, the spatial distribution of inertia is readily achieved. Next, we describe the steps needed in detail:

- **Step 1**: Calculate the power flow to determine the initial conditions of the network (V_{i0} and θ_{i0}), $i = 1, \ldots, n_b$;
- **Step 2**: From the initial conditions, the internal voltage of synchronous generators ($E_i\angle\delta_{i0}$) is calculated using (17), $i = 1, \ldots, n_g$:

$$E_i\angle\delta_i = \left(V_i\angle\theta_i + \frac{Q_i x'_{di}}{V_i\angle\theta_i})\right) + j\frac{P_i x'_{di}}{V_i\angle\theta_i} \tag{17}$$

- **Step 3**: The $D_{j,i}$ element of the **D** matrix is determined from (5) for a configuration with n_g generators. The reduced admittance matrix (internal generator buses) with respect to bus j $\left(Y_j^{\text{red}} \in \mathbb{C}^{(n_g+1)\times(n_g+1)}\right)$ is computed according to the system of equations

$$\begin{bmatrix} I_{G_j} \\ 0 \end{bmatrix} = \begin{bmatrix} Y_{G_jG_j} & Y_{G_jB_j} \\ Y_{B_jG_j} & Y_{B_jB_j} \end{bmatrix} \begin{bmatrix} V_{G_j} \\ V_{B_j} \end{bmatrix} \tag{18}$$

Here, the subscript "G_j" refers to the internal generator buses including system bus j. Additionally, "B_j" refers to system buses except bus j, and the internal generator buses. The solution of (18) is

$$I_{G_j} = Y_j^{\text{red}} V_{B_j} \tag{19}$$

where

$$Y_j^{\text{red}} = Y_{B_jB_j} - Y_{G_jB_j} Y_{B_jB_j}^{-1} Y_{B_jG_j} \tag{20}$$

The equivalent susceptances between the generator k, for $k = 1, \ldots, n_g$, to the disturbed bus j is calculated using the imaginary part of the matrix Y_j^{red}, i.e., $B_{k,j}^j = \text{Im}\{Y_j^{\text{red}}\}_{k,j}$.
- **Step 4**: Using the parameters calculated in the previous steps, the inertia value at bus j is determined by (16). By performing steps 3 and 4 for each bus in the system, we can map the spatial distribution of inertia.

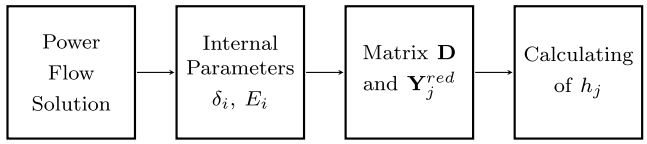

FIGURE 2. Steps to calculate the inertia of a particular bus j.

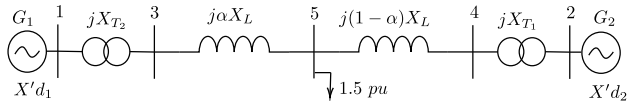

FIGURE 3. 5-bus with 2 generators and a load of 1.5 pu radial system. To achieve a symmetric system α must be 0.5.

Notice that the proposed analytical formulation primarily relies on matrix algebra making our model comprehensible and replicable for planning studies. Furthermore, since our formulation is not an index, it also serves as a benchmark for measurement-based methods.

IV. ANALYSIS AND RESULTS

To validate our analytical formulation illustrated in Fig. 2, we introduce three test systems: (*i*) a radial 5-bus system with two synchronous generators, (*ii*) the IEEE 68-bus system with 16 generators and (*iii*) NPCC 140-bus and 48 generators.

A. RADIAL TEST SYSTEM

The impact of changes in parameters related to the spatial distribution of nodal inertia is analyzed using the 5-bus radial test system illustrated in Figure 3. The two synchronous generators are modeled as a constant voltage source E'_i behind a d-axis transient reactance x'_{d_i}, resulting in a second-order model. The reactances of the transformers are $X_{T_1} = X_{T_2} = 0.1$ pu, while the reactances of the lines and d-axis transient reactance of synchronous generators (100 MW rating) are $X_L = 0.8$ pu, $X'_{d_1} = X'_{d_2} = 0.05$ pu, respectively; all on a common base of 100 MVA.

We investigated the sensitivity of changes in parameters that directly affect the nodal inertia considering three analyses: (*i*) variations in the inertia constant of the generating units and operating conditions, and (*ii*) variations in the electrical distance (reactance) between the generators and buses. Finally, the COI location of a radial system is discussed, and a brief comparison is performed with the simplified inertia distribution model proposed in [15].

1) SENSITIVITY ANALYSIS I

In this section, we apply our method to show how changes in the inertia constant of synchronous machines and the operating point impact the nodal inertia. Firstly, we consider a symmetric network ($\alpha = 0.5$, see Fig. 3) and three cases for the value of the generators' inertia constant. Typical

TABLE 1. Individual inertia constant of generators and the inertia at the COI for the sensitive analysis I studies.

Case	H_1 [s]	H_2 [s]	H_{COI} [s]
I	5	5	10
II	2	5	7
III	5	2	7

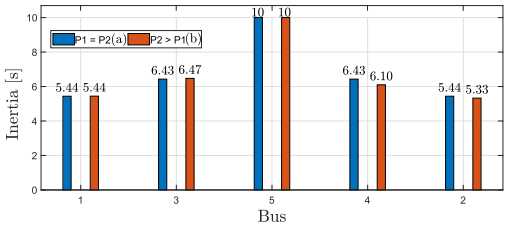

(a) Case I: inertia of buses increases towards Bus 5.

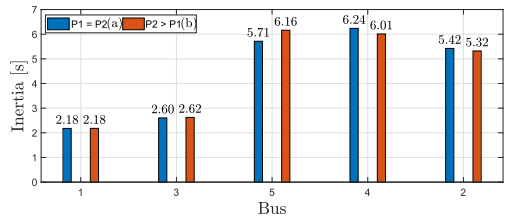

(b) Case II: Bus 4 is the nearest bus to COI.

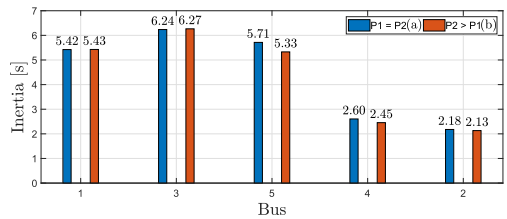

(c) Case III: Bus 3 is the nearest bus to COI.

FIGURE 4. Inertia distribution of the radial system for the three cases analyzed, considering two scenarios for initial operating points.

values of inertia constant and reactances were selected for the radial test system [10], [32]. They are described in Table 1 by case I (symmetric inertia) and cases II and III (uneven inertia). Furthermore, $V_1 = 1.05$ pu, $V_2 = 0.95$ pu, and Bus 1 is the reference ($\theta_1 = 0°$). Also, for each case, two scenarios regarding the initial operating points are considered: (*a*) $P_1 = P_2 = 0.75$ pu, which results in $\delta_1 = 1.91°$, and $\delta_2 = 4.94°$, after the convergence of the power flow; and (*b*) $P_1 = 0.3$ pu, $P_2 = 1.2$ pu, reaching $\delta_1 = 0.76°$, and $\delta_2 = 44°$. Thus, the operating point (b) presents a more significant angle deviation between the generating buses than (a).

Figure 4 shows the inertia distribution for the radial system in each case, considering the nodal inertia values obtained for all system buses with our analytical formulation. Notice that scenario (*a*) are represented by blue bars, whereas scenario (*b*) is by red bars. The step-by-step formulation to determine the nodal inertia for the radial system is presented in Appendix A.

In case I, as shown in Fig. 4(a), the nodal inertia increases towards Bus 5, which presents the highest inertia value ($h_5 = 10$ s). Furthermore, the inertia of Bus 5 is exactly the inertia of the system COI, that is, the sum of H_1 and H_2.

TABLE 2. Inertia constant of each generator and the inertia at the COI to analyze the impact of network topology on the system's COI location.

Case	H_1 [s]	H_2 [s]	H_{COI} [s]
IV	5	10	15
V	10	5	15
VI	7.5	7.5	15

In addition, the inertia of the generator buses (Buses 1 and 2) are slightly higher than their inertia constant (5 s). Therefore, despite the electrical distance between the generators, a mutual contribution influences the nodal inertia values of the generator buses. In cases II (Fig. 4(b)) and III (Fig. 4(c)), the total system inertia is 7 s, and the COI does not match any bus. The bus with the highest inertia is shifted to the right or left towards the generator with the higher inertia constant, that is, Bus 4 for case II, and Bus 3 for case III. In all three cases, the results of the two initial operating point scenarios are quite close, corroborating a minimal influence on the nodal inertia values. In contrast, the generators' inertia constant and the electrical distance are crucial parameters for mapping the values of the distributed inertia. Next, we consider some changes in the system reactances to evaluate the impact of electrical distances on the inertia distribution.

2) SENSITIVITY ANALYSIS II

Here, the impact of the electrical distance (reactance) between the generators and buses on the nodal inertia is analyzed. By varying parameter α, as shown in Fig. 3, it is possible to change the electrical distance between the generators and Bus 5. In this sense, the nodal inertia of Bus 5 can be calculated using (16) and considering the variation of α in the range [0, 1.0]. Furthermore, three additional cases are introduced according to Table 2, considering the same inertia at the COI in all cases ($H_{COI} = 15$ s).

The nodal inertia of Bus 5 as a function of α values is shown in Fig. 5. It is worth noting that, for all cases, there is an α value (α^*) where the nodal inertia at Bus 5 reaches its maximum value ($h_5[\alpha^*] = 15$ s), making Bus 5 the system COI. For the case where the generators have the same inertia constant (Case VI), the maximum nodal inertia occurs for a symmetrical system ($\alpha^*_{III} = 0.5$). However, for cases IV and V, we notice that Bus 5 moves toward the generator with the greatest inertia constant ($\alpha^*_I = 0.79$, $\alpha^*_{II} = 0.21$, respectively). Therefore, nodal inertia is significantly affected by the equivalent electrical distances between the bus and inertia providers and their respective inertia responses.

3) PILOT BUS IDENTIFICATION

A direct application of our analytical formulation is the location of the bus with the highest nodal inertia and, consequently, the system COI location (pilot bus) and its true inertia value:

$$H_{COI} = \max(h_i) \quad i \in \{1, \ldots, n_b\} \tag{21}$$

where h_i is the nodal inertia of all system buses, and H_{COI} is the inertia value of the system COI located at bus $k = \arg\max h_i$. It should be noted that the highest value of nodal

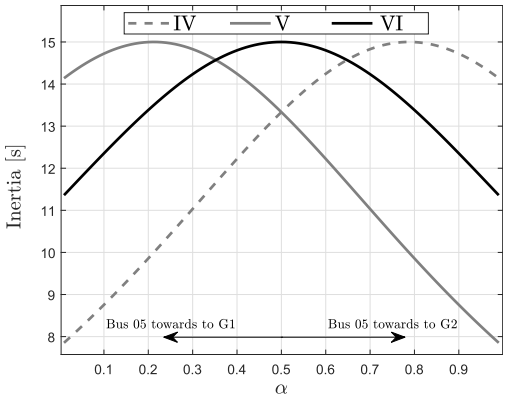

FIGURE 5. Value of inertia at Bus 5 for cases of Table 2 from varying the α parameter to find the COI point, that is, the point of maximum inertia.

TABLE 3. Comparative of nodal inertia obtained for all buses in the radial system (Case III and $\alpha = 0.5$).

Formulation \ Bus	1	2	3	4	5
Proposed	8.118	8.180	9.545	9.757	15.000
From [15]	7.500	7.500	7.500	7.500	7.500

inertia does not necessarily correspond to the sum of the inertia of the sources connected to the system.[1]

For a radial system, such as that shown in Fig. 3, the obtained COI location can be validated analytically. This proof is similar to the example proposed in [34] to determine the bus with COI frequency (3). The comparison is presented in detail in Appendix B, showing that the obtained α^* values that make Bus 5 the highest nodal inertia of the system are the same as those found in [34] which renders the frequency of Bus 5 equal to the COI frequency.

4) COMPARISON WITH [15]

In this section, we compare our method with the one proposed in [15]. We analyze a simple case, which helps compare and reproduce the two methodologies easily. The symmetric radial system ($\alpha = 0.5$) with $H_1 = H_2$ is selected (case VI in Table 2).[2] The nodal inertia of all buses in the system is presented in Table 3.

The results obtained from [15] shown a constant nodal inertia value in all the buses of the system. This clearly indicates that the electrical distance parameters are not properly taken into account in that formulation. On the other hand, the results of the present approach are coherent with the inertia location and weighted by the transmission line and internal generator reactance. The central bus (Bus 5) is the COI of the system given by the total value of inertia available. In the boundaries represented by Buses 1 and 2, the inertia value is slightly higher than the individual generator's inertia. These results are obtained by explicitly including the electrical distance parameters in the proposed formulation.

[1] See Cases II and III for the radial system in Fig. 4.

[2] The frequency divider matrix D for this system is presented in Appendix A.

TABLE 4. Inertia constant of each generating unit considering 100 MVA as system base.

Unit	1	2	3	4	5	6	7	8	9
Inertia [s]	42	30.2	35.8	28.6	26	34.8	26.4	24.3	34.5
Unit	10	11	12	13	14	15	16	NETS	NYPS
Inertia [s]	31	28.2	92.3	496	300	300	450	282.6	647.5

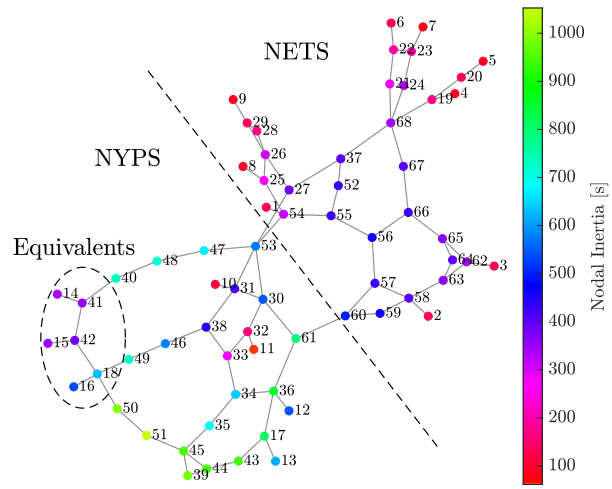

FIGURE 6. Spatial distribution of nodal inertia for the IEEE 68-bus test system.

B. IEEE 68-BUS TEST SYSTEM

The effectiveness of our analytical formulation is tested through the simulations considering the IEEE 68-bus test system. This system includes 16 generators represented by a sixth order model equipped with automatic voltage regulator (AVR) and power system stabilizer (PSS) [36]. Also, the system is divided into five areas: New England transmission system (NETS), New York power system (NYPS), and three areas represented by equivalent generators [36]; all loads are assumed as constant impedance. The individual inertia constant of generators and the total inertia for the areas NETS and NYPS are shown in Table 4.

Following the steps introduced in Fig. 2, the spatial distribution of nodal inertia is accessed after calculating the nodal inertia value of all load buses. Figure 6 illustrates the obtained results. The lowest nodal inertia values in NETS area are located at Buses 20 and 29 ($h_{20} = 139.5$ s and $h_{29} = 140.9$ s), which are also the lowest nodal inertia values in the system. The buses with the highest nodal inertia in the NETS area are 60 and 59, with $h_{60} = 514.5$ s and $h_{59} = 481.0$ s, respectively. These two buses are directly coupled to the interconnection between the NETS and NYPS areas (line 60-61), and thus, their nodal inertia level are influenced by the generators with higher inertial response within NYPS area.

Note that the buses with the highest nodal inertia values (green color) are all in the NYPS area. For instance, Buses 51 and 50 achieve the highest value of nodal inertia ($h_{51} = 1061.0$ s and $h_{50} = 1011.0$ s) between all system buses. Contrarily, Buses 32 and 33, reach the lowest inertia values in the NYPS area, with $h_{32} = 161.3$ s and $h_{33} = 282,7$ s, respectively. We can notice a more uneven spatial distribution

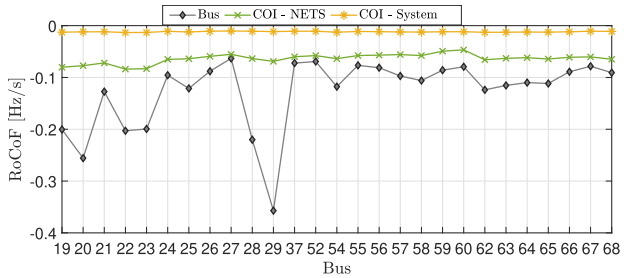

(a) RoCoF Analysis - NETS Area.

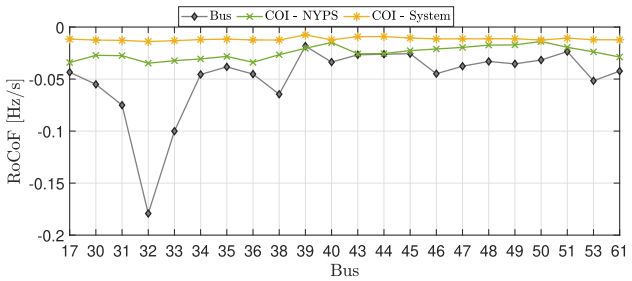

(b) RoCoF Analysis - NYPS Area.

FIGURE 7. Estimation of local RoCoFs after the disturbance applied at each load bus.

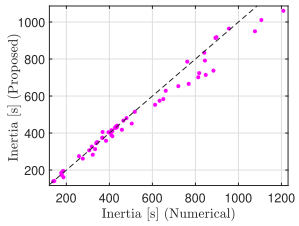

(a) Analytical vs numerical (2nd-order generator model) .

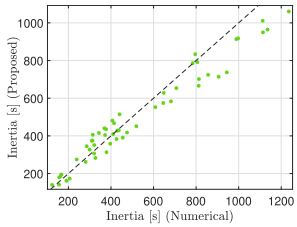

(b) Analytical vs numerical (6th-order generator model).

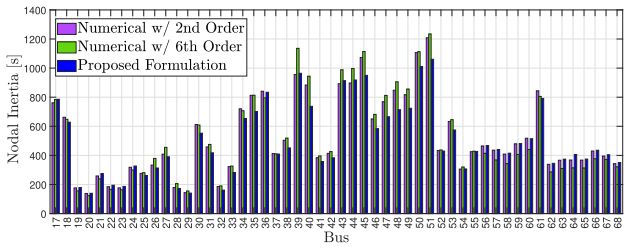

(c) Nodal inertia values from the analytical and numerical (2nd and 6th-order synchronous generator model) methods.

FIGURE 8. Scatter plots (a) and (b) relates the nodal inertia values from the proposed analytical and numerical methods presented in (c) for the IEEE 68-bus test system.

of nodal inertia within NYPS area, with locations with the highest nodal inertia and locations among the lowest.

1) PILOT BUS IDENTIFICATION

Based on the obtained spatial distribution of nodal inercia, no bus matched the total inercia of the system ($H_{COI} = 1,980.1$ s). This is to be expected, as the system is meshy and owing to the distribution of generators. In this case, the pilot bus for the entire system is 51, that is, the bus with the highest nodal inertia in the system. However, since we are able to determine the nodal values of inertia, it is possible to find the nearest bus from the regional COI for each area: (i) NETS: Bus 21 ($h_{21} = 275.0$ s), (ii) NYPS: Bus 34 ($h_{34} = 653.6$ s).

2) NUMERICAL VALIDATION OF THE INERTIA DISTRIBUTION

To validate the obtained results for the meshed system, several nonlinear time-domain simulations are carried out using ANATEM from CEPEL [37]. To determine the local RoCoF, a load step of 100 MW is applied at each load bus (Bus 17 to 68), resulting in a total of 52 time-domain simulations. Despite the magnitude of the disturbance selected as 100 MW, during the time-domain simulations this values varies by the disturbance location. For each simulation, the local RoCoF of the disturbed bus is calculate using a 500 ms time window. Figure 7 points out the estimations of the local RoCoF for all load buses. Fig. 7(a) shows the local RoCoF in NETS area, where Buses 20 and 29 have the highest RoCoF magnitude, which is consistent with the results of Fig. 6. Similarly, Buses 32 and 33 have the highest RoCoF magnitude in the NYPS area, confirming that these buses are located in a location with a lack of inertial response.

In order to validate the obtained nodal inertia values, we can use the estimation of the local RoCoF and the magnitude of each disturbance to numerical estimate the nodal inertia through the underlying formulation in (6). Since the generator model directly affect the simulations and, consequently, the estimation of RoCoF, we consider the second- and sixth-order model of synchronous generator to numerical estimate the nodal inertia and compare with our analytical model.

The results are summarized on Fig. 8. Particularly, Figs. 8(a) and 8(b) shows that the nodal inertia from the analytical and numerical methods are pretty close for values of nodal inertia below than 600 s. As shows Fig. 8(c), the value of nodal inertia for the buses with higher nodal inertia are more conservative regarding our analytical formulation, which does not affect the awareness of the spatial distribution of inertia. It is worth emphasizing that the RoCoF estimation has inherent drawbacks, as the setting of an adequate window, which could figure up errors in the estimated nodal inertia values [38].

C. NPCC 140-BUS

We consider the Northeast Power Coordinating Council (NPCC) 140-bus with 48 generators and 233 transmission lines test system to demonstrate the scalability of our methodology [39]. Table 5 shows the inertia constant of synchronous generators. Following the steps presented in Figure 2, the distribution of nodal inertia is depicted in Figure 9. High nodal inertia values are noticed in Buses 39, 73, 74, 75, 76, 77, 81, 125, and 126, reaching a maximum in Buses 73 and 75, with 1,469.5 s and 1,465.2 s, respectively. Low nodal inertia buses are distributed across the system, particularly at boundaries. Bus 136 has the lowest nodal inertia between the load buses, with 68.16 s, due to the influence of the low nodal inertia of the generating Bus 137.

To validate the obtained distribution of nodal inertia, we select a region with unequal nodal inertia distribution,

TABLE 5. Inertia constant of each generating unit considering 100 MVA as system base - NPCC 140-bus.

Unit	36	21	22	23	23	24	25	26	27
Inertia [s]	30.3	34.8	28.6	7.34	18.6	34.8	26.4	34.2	24.3
Unit	42	47	48	50	51	53	54	54	55
Inertia [s]	18.86	15.17	15.17	34.44	21.46	37	51.24	51.24	59.78
Unit	56	57	60	61	65	68	71	72	78
Inertia [s]	21.94	17.71	21.74	8.32	10.71	3.77	8.5	11.77	1000
Unit	79	80	82	101	86	91	92	97	98
Inertia [s]	48	23.80	19.60	55	79	98.70	27	36	72
Unit	115	119	120	121	122	123	130	133	134
Inertia [s]	46	30	1000	66	190	33	24	1000	44
Unit	135	137	139						
Inertia [s]	115	3.5	1000						

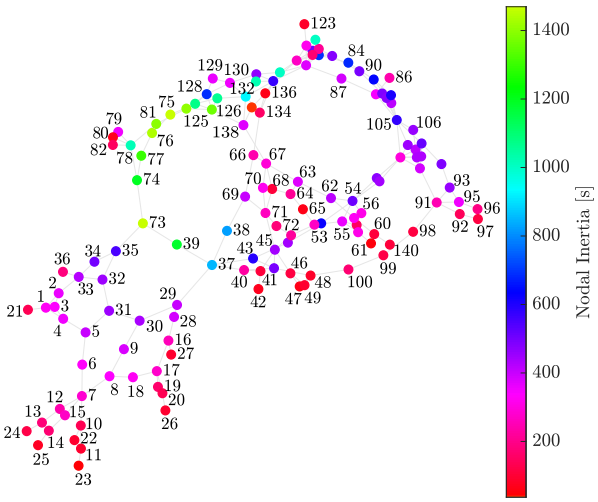

FIGURE 9. Spatial distribution of nodal inertia for the NPCC 140-bus system.

highlighted with a dashed line in Figure 9, to perform the frequency response analysis of individual buses. Figure 10 shows the frequency response and RoCoF estimation considering a load step of 100 MW applied at Buses 75, 132, 128, 138, and 136. Previous colors defined for buses in Figure 9 are again applied to facilitate the understanding. Note that Buses 136 and 138 are more prone to have higher RoCoF, corroborating our results that these buses have low nodal inertia (less than 400 s). Also, Bus 75 has fewer frequency deviations, resulting in higher nodal inertia (greater than 1400 s) according to our analytical formulation.

V. COMPARATIVE ANALYSIS

In this section, we compare the results obtained using our analytical formulation with those from two methodologies proposed in the literature. In addition, we provide an asymptotic analysis regarding the concept of slow coherence areas, introducing the interpretation of the spatial distribution of inertia from the point of view of the coherence of generators and buses. In this section, we use the IEEE 68-bus system, which is the benchmark system widely used in the literature.

A. INERTIA DISTRIBUTION METHODOLOGIES COMPARISON

The first method, introduced in [23], proposes an index based on modal analysis to obtain a spatial distribution of inertia. By contrast, [20] designed an index based on time-domain

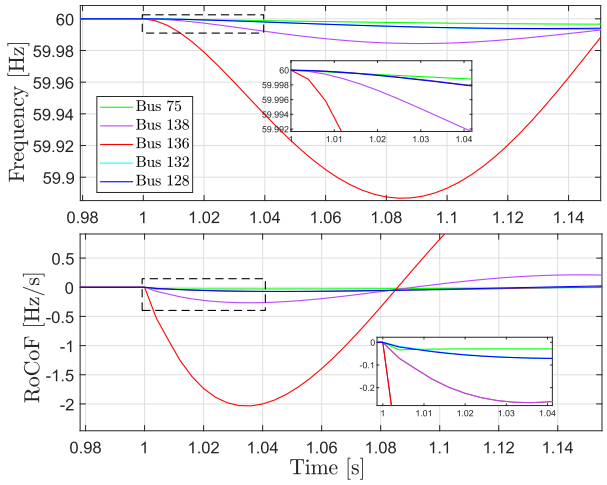

FIGURE 10. Frequency Response and Estimation of RoCoF dynamics considering the first second after a load step applied to Buses 75, 132, 18, 138 and 136.

simulations. Because these methodologies rely on indexes, they are incapable of explicitly determining the values of inertia at each bus in the system. Thus, a comparative analysis should consider the ranking of the buses based on their nodal inertia levels.

1) MODAL ANALYSIS-BASED INDEX

Following [23], we consider the linearized power system model to obtain the network sensitivities (C_θ), which is the sensitivity of bus voltage angles with respect to changes in the state variables ($\Delta\omega$, $\Delta\delta$), and the system modeshapes (Φ). The inertia distribution is determine through the network modeshape (S_θ), that is, the product of the network sensitivities by a particular modeshape ($C_\theta \cdot \Phi_j$).

The IEEE 68-bus system presents four inter-area modes. The network modeshape is calculated for each inter-area mode, as shown in Fig. 11. For each inter-area mode there is a bus that indicates the center of oscillation: Bus 50 for the modes 0.38 Hz and 0.5 Hz, and the Buses 53 and 54 for modes 0.79 Hz and 0.59 Hz, respectively. However, to determine the nodal inertia distribution using this approach, it is necessary to define the critical/dominant inter-area mode. As presented in [23], the critical mode corresponds to the one with 0.38Hz, and can be obtained through the localness index proposed by [40]. Therefore, the mapping of nodal inertia distribution should be calculated using this mode.

2) TIME-DOMAIN-BASED INDEX

Authors [20] and [21] propose an index considering the distance between each bus frequency and the COI frequency after a disturbance. The distance are calculate using (22)

$$d_j = \int_{t_0}^{T+t_0} \left(f_j(k) - f_{COI}(k)\right)^2 dk \tag{22}$$

where t_0 is the time of disturbance and T is the parsed window size. The distances are normalized with respect to the highest value, defining the inertia distribution index (IDI).

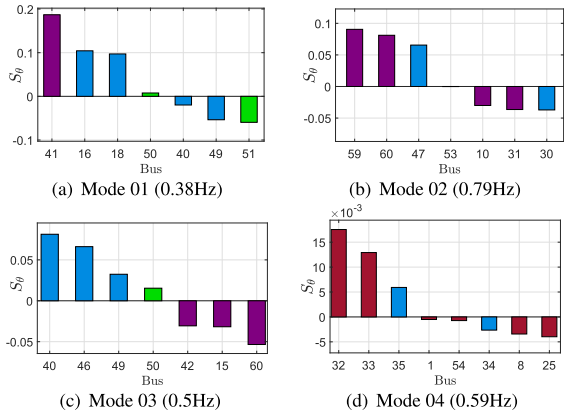

FIGURE 11. Network modeshapes (S_θ) of all inter-area modes considering only buses around the center of oscillations for better visualization.

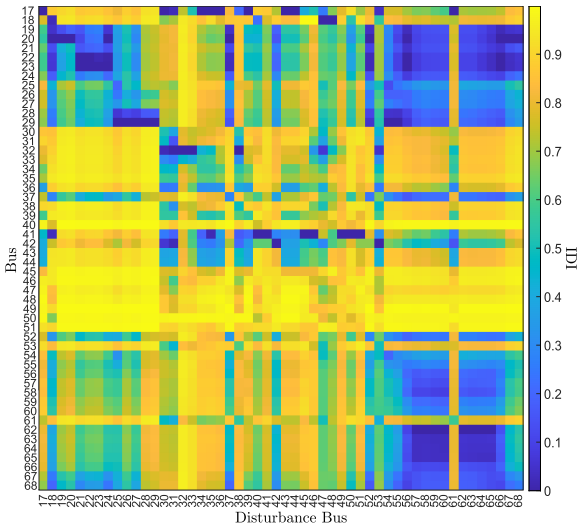

FIGURE 12. Time-domain-based index calculated for all load buses considering the disturbances applied at each bus.

To better visualization, we calculate the value of $1 - IDI$, that is,the buses closest to the system COI have an index close 1, whereas buses furthest have an index close to 0. Figure 12 shows the IDI calculated for the IEEE 68-bus test system considering a disturbance of 100 MW applied at all load buses. We can notice that there are some location with the inertial index closest to 1 for all the disturbances, for instance, Buses 48-50. However, in several locations the index varies according to the disturbance location. Therefore, to compare with our analytical formulation, we should consider the critical case depicted in the main diagonal elements of Fig. 12, that is, the calculated index for a particular bus when the disturbance is applied to it.

3) ANALYTICAL VS INDEX-BASED METHODS

Here, we compare the nodal inertia distribution using our formulation with the above indexes. Figure 13 shows the nodal inertia ranking, where position 1 of the ranking represents the bus with the highest nodal inertia and position 52 represents the bus with the lowest nodal inertia. The modal-based and

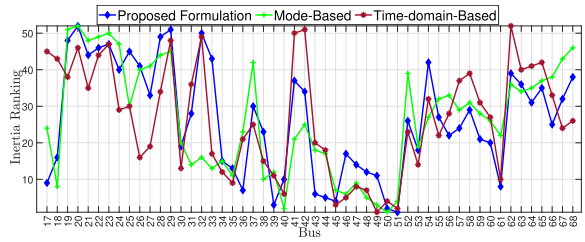

FIGURE 13. Inertia ranking of load buses considering our formulation and two index-based methods.

time-domain-based indexes are compared in terms of critical mode and critical disturbance, respectively.

Regarding the highest and lowest nodal inertia buses, both indexes are in accordance with the obtained nodal inertia values. For instance, a low nodal inertia index was obtained for Buses 20, 22, 23, and 29 within the NETS area, and a high nodal inertia index for Buses 40, 45, 50, and 51 within the NYPS area. However, for some locations, the results from the index-based methods deviate from the obtained nodal inertia values. For instance, while index-based methodologies suggest high nodal inertia in Buses 32 and 33, our proposed formulation properly shows a lack of inertial response in this location. This behavior can be explained by the observation of local oscillations.

The modal-based analysis depends on the critical inter-area mode (0.38 Hz), which comprises generators of the NETS and NYPS areas that oscillate against equivalent generators 14, 15, and 16. However, in the NYPS area, there is a local oscillation mode (1.8 Hz) related to generator 11. This local mode impacts the frequency behavior of Buses 32 and 33 after a local disturbance, resulting in faster frequency oscillations (see the local RoCoF in Fig.7(b)). The time-domain-based index properly reflects the low nodal inertia of Bus 32; however, the ranking of Bus 33 indicates high nodal inertia. These differences can be understood as numerical issues in obtaining the index.

In conclusion, unlike the existing inertia distribution indexes, our straightforward analytical formulation properly reflects the locational inertial response, independent of time-domain simulations or the analysis of oscillation modes. Additionally, we calculated all nodal inertia values in less than 140 ms, following the four steps described in III-B, avoiding running and analyzing successive time-domain simulations.[3] Also, our proposed analytical formulation is suitable as a reference model for comparison with other inertia distribution indexes based on measurements.

B. INERTIA DISTRIBUTION AND SLOW COHERENCY AREAS

Slow coherency is an analytical method to determine the coherent machines based on the lower frequency inter-area mode, where a group of coherent machines oscillates against another coherent group [41]. This concept can be extended to

[3] All simulations were carried out in MATLAB R2018a on an Intel Core i5-8265U 2.00 GHz processor with 8 GB of memory.

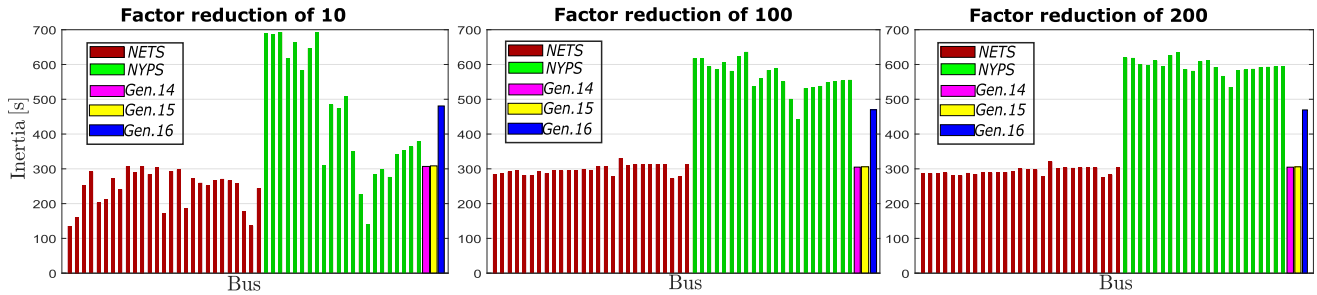

FIGURE 14. Inertia distribution of IEEE 68-Bus System considering three scenarios of reduction of internal reactances of the coherent areas.

non generating buses, to group all system buses into coherent areas. The frequency response on all the buses in the coherent area is considered in unison, which means that in the ideal case, all the reactances within a coherent area are close to zero (infinite admittances), keeping the reactances of lines connecting different coherent areas the same.

In this sense, we can obtain the inertia distribution for this edge case using our proposed formulation. For the IEEE 68-Bus system, the coherent areas obtained by the slow coherency method are the five areas: NETS, NYPS, Gen. 14, Gen. 15, and Gen. 16 [42]. Accordingly, the internal reactances of these five areas are reduced by factors of: 10, 100, and 200. For all these cases, the internal reactances of generators are reduced by 10. The line reactances of the lines 60-61, 25-53, 54-53, 40-41, 41-42, 42-18, 49-18, and 50-18 connecting different areas are kept constant. Figure 14 shows the inertia distribution obtained for the three cases detailed above.

We can observe that, as expected by the slow coherency method, the inertias of buses within a coherent area converge to the same values, the total inertia of the respective area (see the Table 4), as the internal reactances are reduced. Therefore, our inertia distribution formulation is supported by an asymptotic analysis and consistent with the coherent areas. Furthermore, our inertia distribution formulation can more accurately reveal the coherence of the buses, taking into account the cases in which the internal reactances of the areas are far from zero, that is, the base case.

VI. DISCUSSION

By mapping the nodal inertia using our analytical formulation, system operators can accurately and quickly identify critical regions to take local preventive actions, helping in the operational planning process. We summarize some potential applications arising from the knowledge of the distribution of nodal inertia below.

- The locational inertial response can be improved in low-inertia nodes by placing synchronous compensators or IBRs supplying virtual inertia.
- As a byproduct of determining nodal inertia values, system operators can identify the system or regional COI, that is, the pilot buses, to measure the frequency response. These measurements are essential for designing special protection schemes and controls.

TABLE 6. Power flow for the radial system with $\alpha = 0.5$ and $P_1 = P_2 = 0.75$ pu.

Bus	1	2	3	4	5
V	1.05	0.95	1.0102	0.9276	0.9111
θ	0	2.5958	-4.0548	-2.2865	-23.0788

- The scheduling of units can consider the impact of generators and transmission lines on the local frequency response. The proposed methodology can be embedded in a scheduling problem to optimally determine the least cost operation ensuring locational system security.

VII. CONCLUSION

This paper proposes a novel analytical formulation that relies only on steady-state parameters for determining the nodal inertia value and attaining the spatial distribution of inertia in a power system. The analyses carried out in the radial test system, varying the generators' inertia constant and network topology, show that our formulation adequately quantifies the spatial distribution of inertia. Time-domain simulations and numerical estimations support the nodal inertia values obtained by considering the meshed IEEE 68-bus and the large interconnected NPCC 140-bus system. The comparative analysis against existing inertia distribution indexes highlights the strengths of our analytical formulation considering meshed systems with several inter-area and local modes. In addition, slow coherency analysis provides additional validation for the proposed formulation and an innovative interpretation of the spatial distribution of inertia. Future work will focus on including our formulation in the scheduling problem to optimally determine the need for inertial resources to support decision-making.

APPENDIX. A) NODAL INERTIA FOR THE RADIAL SYSTEM

Following the steps of Fig.2, the distribution of nodal inertia for the radial system in Fig. 3 with $\alpha = 0.5$ and $P_1 = P_2 = 0.75$ pu can be determined. The system operating point (voltage and angle) is obtained by solving the AC power flow. Table 6 summarizes the results. Next, synchronous machine internal voltage (E_i) and angle (δ_i) are obtained as $E_1 = 1.0718$ pu, $E_2 = 0.9637$ pu, $\delta_1 = 1.9096°$, $\delta_2 = 4.9433°$.

Frequency divider matrix ($\mathbf{D}$) is determined in (23) and the reduced admittance matrix (Y^{red}) in (24). Notice that

each row of (24) is calculated using (20), and thus, (24) includes the equivalent susceptancies between each generator and bus. For example, $B_{1,5} = \text{Im}\{Y^{red}\}_{1,5}$ is the equivalent susceptance between generator 01 and Bus 5.

$$D = \begin{bmatrix} 0.9545 & 0.0455 \\ 0.0455 & 0.9545 \\ 0.8636 & 0.1364 \\ 0.1364 & 0.8636 \\ 0.5000 & 0.5000 \end{bmatrix} \tag{23}$$

$$Y^{red} = \begin{bmatrix} 20 & 0.7781 \\ 0.7781 & 20 \\ 6.6667 & 0.8958 \\ 0.8958 & 6.6667 \\ 1.8182 & 1.8182 \end{bmatrix}^T \tag{24}$$

Finally, using the inertia constant of synchronous generators, the nodal inertia for all system buses is calculated through (16). For the radial system, given a bus j, the nodal inertia is determined according to (25).

$$h_j = \frac{B_{1,j}E_1 \cos\left(\delta_{10} - \theta_{j0}\right) + B_{2,j}E_2 \cos\left(\delta_{20} - \theta_{j0}\right)}{\frac{D_{j,1}}{H_1}B_{1,j}E_1 \cos\left(\delta_{10} - \theta_{j0}\right) + \frac{D_{j,2}}{H_2}B_{2,j}E_2 \cos\left(\delta_{20} - \theta_{j0}\right)} \tag{25}$$

APPENDIX. B) COI IDENTIFICATION IN A RADIAL SYSTEM

To check the consistency of the obtained α^* values, we use the frequency divider formulation (4), and the underlying COI equation (3) [34]. Using equation (4), the frequency of Bus 5 is:

$$\Delta f_5 = \frac{X_{52'}}{X_{51'} + X_{52'}}\Delta\omega_1 + \frac{X_{51'}}{X_{51'} + X_{52'}}\Delta\omega_2 \tag{26}$$

where $X_{51'}$ and $X_{52'}$ are the total reactances between Bus 5 and the internal buses of generators 1 and 2, respectively:

$$X_{51'} = X'_{d_1} + X_{T_1} + \alpha X_L \tag{27}$$

$$X_{52'} = X'_{d_2} + X_{T_2} + (1-\alpha)X_L \tag{28}$$

By equation (3), the COI frequency is

$$\Delta f_{COI} = \frac{H_1}{H_1 + H_2}\Delta\omega_1 + \frac{H_2}{H_1 + H_2}\Delta\omega_2 \tag{29}$$

Comparing the terms of (26) with those of (29), it is possible to determine the values of reactances that make the frequency of the bus equal to the frequency of the COI ($\Delta f_5 = \Delta\omega_{COI}$) as

$$X_{51'} = \frac{H_2}{H_1+H_2}[(X'_{d_1}+X'_{d_2}) + (X_{T_1}+X_{T_2})+X_L)] \tag{30}$$

$$X_{52'} = \frac{H_1}{H_1+H_2}[(X'_{d_1}+X'_{d_2})+(X_{T_1}+X_{T_2})+X_L)] \tag{31}$$

Finally, the value of α^* can be achieved by substituting (27) on the left-hand side of (30):

$$\alpha^* = \frac{H_2(X'_{d_2} + X_{T_2} + X_L) - H_1(X'_{d_1} + X_{T_1})}{(H_1 + H_2)X_L} \tag{32}$$

TABLE 7. α^* values for bus 5.

Eq.	(a)	(b)	(c)
(16)	0.790	0.210	0.500
(32)	0.792	0.208	0.500

Table 7 shows a comparison between the values of α^* provided by our analytical formulation with those obtained using (32). There are no sharp differences in the results, which validates the proposed formulation also for the COI identification for a radial system.

REFERENCES

[1] F. Milano, F. Dorfler, G. Hug, D. J. Hill, and G. Verbic, "Foundations and challenges of low-inertia systems (invited paper)," in *Proc. Power Syst. Comput. Conf. (PSCC)*, Jun. 2018, pp. 1–25.

[2] L. Pagnier and P. Jacquod, "Inertia location and slow network modes determine disturbance propagation in large-scale power grids," *PLoS ONE*, vol. 14, no. 3, pp. 1–17, Mar. 2019.

[3] A. Ulbig, T. S. Borsche, and G. Andersson, "Impact of low rotational inertia on power system stability and operation," *IFAC Proc. Vols.*, vol. 47, no. 3, pp. 7290–7297, 2014.

[4] D. Doheny and M. Conlon, "Investigation into the local nature of rate of change of frequency in electrical power systems," in *Proc. 52nd Int. Universities Power Eng. Conf. (UPEC)*, Aug. 2017, pp. 1–6.

[5] L. R. Gorjão, R. Jumar, H. Maass, V. Hagenmeyer, G. C. Yalcin, J. Kruse, M. Timme, C. Beck, D. Witthaut, and B. Schäfer, "Open database analysis of scaling and spatio-temporal properties of power grid frequencies," *Nature Commun.*, vol. 11, no. 1, p. 6362, Dec. 2020.

[6] P. Wall, N. Shams, V. Terzija, V. Hamidi, C. Grant, D. Wilson, S. Norris, K. Maleka, C. Booth, Q. Hong, and A. Roscoe, "Smart frequency control for the future GB power system," in *Proc. IEEE PES Innov. Smart Grid Technol. Conf. Eur. (ISGT-Europe)*, Oct. 2016, pp. 1–6.

[7] S. You, H. Li, S. Liu, K. Sun, W. Wang, W. Qiu, and Y. Liu, "Calculate center-of-inertia frequency and system RoCoF using PMU data," in *Proc. IEEE Power Energy Soc. Gen. Meeting (PESGM)*, Jul. 2021, pp. 1–5.

[8] M. Sun, G. Liu, M. Popov, V. Terzija, and S. Azizi, "Underfrequency load shedding using locally estimated RoCoF of the center of inertia," *IEEE Trans. Power Syst.*, vol. 36, no. 5, pp. 4212–4222, Sep. 2021.

[9] B. A. Osbouei, G. A. Taylor, O. Bronckart, J. Maricq, and M. Bradley, "Impact of inertia distribution on power system stability and operation," in *Proc. IEEE Milan PowerTech*, Jun. 2019, pp. 1–6.

[10] B. Tan, J. Zhao, M. Netto, V. Krishnan, V. Terzija, and Y. Zhang, "Power system inertia estimation: Review of methods and the impacts of converter-interfaced generations," *Int. J. Electr. Power Energy Syst.*, vol. 134, Jan. 2022, Art. no. 107362.

[11] P. M. Ashton, C. S. Saunders, G. A. Taylor, A. M. Carter, and M. E. Bradley, "Inertia estimation of the GB power system using synchrophasor measurements," *IEEE Trans. Power Syst.*, vol. 30, no. 2, pp. 701–709, Mar. 2015.

[12] D. Wilson, J. Yu, N. Al-Ashwal, B. Heimisson, and V. Terzija, "Measuring effective area inertia to determine fast-acting frequency response requirements," *Int. J. Electr. Power Energy Syst.*, vol. 113, pp. 1–8, Dec. 2019. [Online]. Available: https://www.sciencedirect.com/science/article/pii/S0142061519304892

[13] S. You, Y. Liu, G. Kou, X. Zhang, W. Yao, Y. Su, S. W. Hadley, and Y. Liu, "Non-invasive identification of inertia distribution change in high renewable systems using distribution level PMU," *IEEE Trans. Power Syst.*, vol. 33, no. 1, pp. 1110–1112, Jan. 2018.

[14] N. Ma and D. Wang, "Extracting spatial–temporal characteristics of frequency dynamic in large-scale power grids," *IEEE Trans. Power Syst.*, vol. 34, no. 4, pp. 2654–2662, Jul. 2019.

[15] F. Zeng, J. Zhang, Y. Zhou, and S. Qu, "Online identification of inertia distribution in normal operating power system," *IEEE Trans. Power Syst.*, vol. 35, no. 4, pp. 3301–3304, Jul. 2020.

[16] V. Trovato, "The impact of spatial variation of inertial response and flexible inter-area allocation of fast frequency response on power system scheduling," *Electr. Power Syst. Res.*, vol. 198, Sep. 2021, Art. no. 107354.

[17] M. Tuo and X. Li, "Security-constrained unit commitment considering locational frequency stability in low-inertia power grids," *IEEE Trans. Power Syst.*, early access, Oct. 19, 2022, doi: 10.1109/TPWRS.2022.3215915.

[18] L. Pagnier and P. Jacquod, "Optimal placement of inertia and primary control: A matrix perturbation theory approach," *IEEE Access*, vol. 7, pp. 145889–145900, 2019.

[19] M. Tuo and X. Li, "Optimal allocation of virtual inertia devices for enhancing frequency stability in low-inertia power systems," in *Proc. North Amer. Power Symp. (NAPS)*, Nov. 2021, pp. 1–6.

[20] H. Pulgar-Painemal, Y. Wang, and H. Silva-Saravia, "On inertia distribution, inter-area oscillations and location of electronically-interfaced resources," *IEEE Trans. Power Syst.*, vol. 33, no. 1, pp. 995–1003, Jan. 2018.

[21] Y. Wang, H. Silva-Saravia, and H. Pulgar-Painemal, "Estimating inertia distribution to enhance power system dynamics," in *Proc. North Amer. Power Symp. (NAPS)*, Sep. 2017, pp. 1–6.

[22] L. Hu, Y. Li, W. Wang, Y. Tan, Y. Cao, and K. Y. Lee, "Inertia estimation of power grid with VSC-MTDC system," *IFAC-PapersOnLine*, vol. 51, no. 28, pp. 197–202, 2018.

[23] D. Brahma and N. Senroy, "Sensitivity-based approach for assessment of dynamic locational grid flexibility," *IEEE Trans. Power Syst.*, vol. 35, no. 5, pp. 3470–3480, Sep. 2020.

[24] D. Brahma and N. Senroy, "Spatial distribution of grid inertia and dynamic flexibility: Approximations and applications," *IEEE Trans. Power Syst.*, vol. 36, no. 4, pp. 3465–3474, Jul. 2021.

[25] W. J. Farmer and A. J. Rix, "Evaluating power system network inertia using spectral clustering to define local area stability," *Int. J. Electr. Power Energy Syst.*, vol. 134, Jan. 2022, Art. no. 107404.

[26] J. H. Chow, A. Chakrabortty, L. Vanfretti, and M. Arcak, "Estimation of radial power system transfer path dynamic parameters using synchronized phasor data," *IEEE Trans. Power Syst.*, vol. 23, no. 2, pp. 564–571, May 2008.

[27] Y. Wang, H. Silva-Saravia, and H. Pulgar-Painemal, "Actuator placement for enhanced grid dynamic performance: A machine learning approach," *IEEE Trans. Power Syst.*, vol. 34, no. 4, pp. 3119–3128, Jul. 2019.

[28] D. A. Kez, A. M. Foley, and D. J. Morrow, "Analysis of fast frequency response allocations in power systems with high system non-synchronous penetrations," *IEEE Trans. Ind. Appl.*, vol. 58, no. 3, pp. 3087–3101, May 2022.

[29] P. B. Garcia-Rosa, S. D'Arco, and J. A. Suul, "Placement of virtual inertia from HVDC terminals based on a frequency deviation index," in *Proc. IEEE Madrid PowerTech*, Jun. 2021, pp. 1–7.

[30] L. Vanfretti and J. H. Chow, "Analysis of power system oscillations for developing synchrophasor data applications," in *Proc. IREP Symp. Bulk Power Syst. Dyn. Control VIII (IREP)*, Aug. 2010, pp. 1–17.

[31] F. Milano and A. Ortega, "Frequency divider," *IEEE Trans. Power Syst.*, vol. 32, no. 2, pp. 1493–1501, May 2017.

[32] J. H. Chow and J. Sanchez-Gasca, *Power System Modeling, Computation, and Control*, 1st ed. Hoboken, NJ, USA: Wiley, 2020.

[33] P. M. Anderson and A. A. Found, *Power System Control and Stability*, 2nd ed. Hoboken, NJ, USA: Wiley, 1977.

[34] F. Milano and O. M. Álvaro, *Frequency Variations in Power Systems*, 1st ed. Hoboken, NJ, USA: Wiley, 2020.

[35] N. Shams, P. Wall, and V. Terzija, "Active power imbalance detection, size and location estimation using limited PMU measurements," *IEEE Trans. Power Syst.*, vol. 34, no. 2, pp. 1362–1372, Mar. 2019.

[36] C. Canizares, T. Fernandes, E. Geraldi, L. Gerin-Lajoie, M. Gibbard, I. Hiskens, J. Kersulis, R. Kuiava, L. Lima, F. DeMarco, N. Martins, B. C. Pal, A. Piardi, R. Ramos, J. dos Santos, D. Silva, A. K. Singh, B. Tamimi, and D. Vowles, "Benchmark models for the analysis and control of small-signal oscillatory dynamics in power systems," *IEEE Trans. Power Syst.*, vol. 32, no. 1, pp. 715–722, Jan. 2017.

[37] *Análise de Transitórios Eletromecânicos Manual do Usuário*, CEPEL Centro de Pesquisas de Energia Elétrica, Brasília, Brazil, 2020.

[38] Y. Zuo, G. Frigo, A. Derviškadic, and M. Paolone, "Impact of synchrophasor estimation algorithms in ROCOF-based under-frequency load-shedding," *IEEE Trans. Power Syst.*, vol. 35, no. 2, pp. 1305–1316, Mar. 2020.

[39] J. Chow and G. Rogers, "User manual for power system toolbox, version 3.0," 2008. [Online]. Available: https://sites.ecse.rpi.edu/~chowj/PSTMan.pdf

[40] S. Ghosh and N. Senroy, "The localness of electromechanical oscillations in power systems," *Int. J. Electr. Power Energy Syst.*, vol. 42, no. 1, pp. 306–313, Nov. 2012.

[41] J. H. Chow, *Power System Coherency and Model Reduction*, 1st ed. New York, NY, USA: Springer, 2013.

[42] J. H. Chow, *Time-Scale Modeling of Dynamic Networks With Applications to Power Systems*. New York, NY, USA: Springer, 1982.

BRUNO PINHEIRO (Graduate Student Member, IEEE) was born in Manaus, Amazonas, Brazil, in 1997. He received the B.E. degree from the Federal University of Amazonas, Amazonas, in 2018, and the M.Sc. degree in electrical engineering from the University of Campinas, São Paulo, Brazil, in 2021, where he is currently pursuing the Ph.D. degree. His research interests include power system stability and control, modeling, and inertia estimation methods.

LUIGI VIOLA (Graduate Student Member, IEEE) received the B.E. degree from São Paulo State University (UNESP), Guaratinguetá, Brazil, in 2014, and the M.Sc. degree in electrical engineering from the University of Campinas, Brazil, in 2017, where he is currently pursuing the Ph.D. degree. His research interests include power system operation and economics.

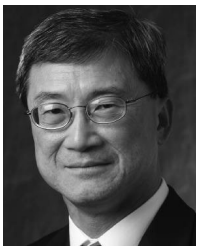

JOE H. CHOW (Life Fellow, IEEE) received the M.S. and Ph.D. degrees from the University of Illinois at Urbana–Champaign, Champaign, IL, USA. After working with the General Electric Power System Business, Schenectady, NY, USA, he joined the Rensselaer Polytechnic Institute, Troy, NY, USA, in 1987, where he is currently an Institute Professor in electrical, computer, and systems engineering. His research interests include power system dynamics and control, FACTS controllers, and synchronized phasor data. He is also a member of the U.S. National Academy of Engineering. He was a past recipient of the IEEE PES Charles Concordia Power Engineering Award and the Outstanding Power Engineering Educator Award.

DANIEL DOTTA (Member, IEEE) received the B.S., M.S., and Ph.D. degrees from the Federal Institute of Santa Catarina, Florianópolis, Brazil, in 2001, 2003, and 2009, respectively. From 2006 to 2015, he was a Professor with the Federal Institute of Santa Catarina. In 2015, he joined the University of Campinas, Campinas, Brazil, where he is currently an Assistant Professor. He also spent two sabbatical leaves as a Visiting Scholar with the Rensselaer Polytechnic Institute, Troy, NY, USA, from 2011 to 2013 and from 2018 to 2019, respectively.